Physics in Medicine 8 (2019) 100020

Contents lists available at ScienceDirect

Physics in Medicine

journal homepage: www.elsevier.com/locate/phmed

Development of a spatially and timely resolved CFD model of a steam sterilizer to predict the load temperature and the theoretical inactivation of bacteria based on sterilization parameters

Manuel Feurhuber[a,*], Paul Burian[a], Marino Magno[b], Marco Miranda[b], Christoph Hochenauer[a]

[a] Institute of Thermal Engineering, Graz University of Technology, Inffeldgasse 25/B, 8010, Graz, Austria
[b] W&H Sterilization, Via Bolgara 2, I-24060, Brusaporto, BG, Italy

ARTICLE INFO

Keywords:
Steam sterilization
Computational fluid dynamics (CFD)
Heat transfer
Inactivation of bacteria
Multiphase flow

ABSTRACT

This paper presents a CFD model to predict the fluid flow, fluid temperature, load temperature and the theoretical inactivation of bacteria in a modern steam sterilizer, with three significant modifications compared to current state-of-the-art simulations of steam sterilizers. 1) The fluid and the load temperature was investigated for unwrapped load. Measurements of the fluid temperature and the load temperature were performed to validate the CFD model. The average error between the simulated and the measured temperatures was below 0.4 K. 2) The steam quality inside a steam sterilizer was investigated for unwrapped load. With the developed CFD model it is possible to predict the steam quality inside the steam sterilizer spatially and temporally resolved. 3) A first order reaction kinetic approach was added to the CFD model to predict the theoretical inactivation of two different types of bacteria in the steam sterilizer, as well as on the surface of the unwrapped load based on sterilization parameters. The results indicate that the CFD model is able to predict the theoretical inactivation of bacteria on the surface of the load, based on sterilization parameters.

1. Introduction

Steam sterilization is commonly used to sterilize scalpels, forceps, tubes and other re-useable medical items. Criteria for an effective sterilization cycle can be found in the European standards [1,2] and in international norms [3]. In general every steam sterilization cycle can be divided into three phases. The pressure profile and fluid temperature of the sterilization cycle researched in this work can be seen in Fig. 1. During the first phase a vacuum pump reduces the pressure in the steam sterilizer to a value of approximately 0.15 bar. Afterwards a steam generator fills the steam sterilizer with steam until the pressure reaches 1.4 bar. The pressure is reduced three times, and raised twice during this initial phase, the aim of which is to remove all non-condensable gases (NCGs) from the steam sterilizer. In the second phase the steam sterilizer raises the pressure from 0.3 bar to the sterilization plateau of approximately 3.2 bar. Following the pressure increase, regulations demand a pressure hold for a pre-defined time. During that phase the sterilization takes place. This phase of the steam sterilization cycle was investigated in this study (see Fig. 1). In the third phase a vacuum pump is used to reduce the pressure. The aim of the third phase is to dry and cool down the load. At the end of the sterilization cycle the steam sterilizer is filled with ambient air to guarantee a safe opening of the door.

The working principle of a steam sterilizer is based on the high heat transfer rates from the steam to the load. These high heat transfer rates result due to condensation from the steam on the surface of the medical equipment. In this way, the surface temperature of the medical equipment nearly reaches the saturation temperature of the steam. These high surface temperatures compared with high dwell times of these temperatures are beneficial to inactivate the bacteria on the surface of the load. To guarantee these high heat transfer rates, all NCGs must be removed from the steam sterilizer [4].

In the past a wide area of researchers investigated the steam sterilization cycle experimentally. Lapanaitis et al. [5], for example, investigated the relation between the length of the steam sterilization cycle and the weight of the load. Many other authors investigated the air removal and steam penetration into hollow loads (helix tests) [6–9]. The work of Kaiser [10] shows the influence of the non-condensable gases (NCGs) on the steam sterilization cycle.

In contrast, few articles have been published that investigate steam sterilization cycles numerically. Lau et al. developed a 1-D numerical model to simulate the temperatures in a steam sterilizer [11] as well as

* Corresponding author.
E-mail address: manuel.feurhuber@tugraz.at (M. Feurhuber).

https://doi.org/10.1016/j.phmed.2019.100020
Received 18 March 2019; Received in revised form 12 November 2019; Accepted 20 November 2019
Available online 29 November 2019

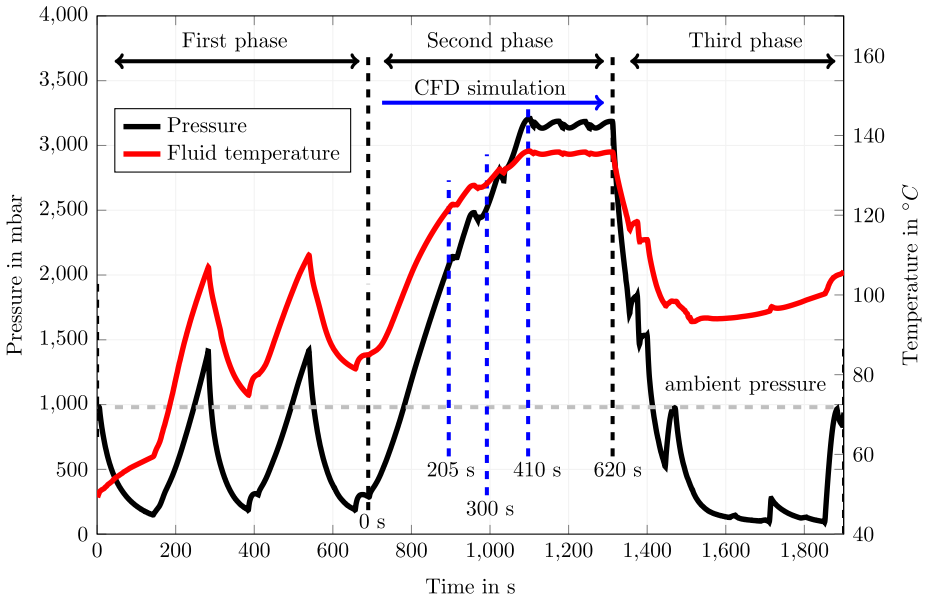

Fig. 1. Measured pressure and fluid temperature in the steam sterilizer during a sterilization cycle. First phase: Removal of the air; Second phase: Sterilization; Third phase: Drying and cooling.

the load temperature [12]. Feurhuber et al. [13] developed a CFD model to predict the fluid temperature, as well as the load temperature in a steam sterilizer for wrapped load. Furthermore research of Feurhuber et al. [14] investigated the air-removal and the steam penetration inside hollow loads (helix tests). In a third publication the Feurhuber et al. [15] investigated the NCGs in vacuum and non-vacuum steam sterilizers using CFD.

In this study the 1) the fluid temperature and the load temperature was investigated for unwrapped load, 2) the steam quality in a steam sterilizer with unwrapped load was investigated and 3) the theoretical inactivation of two different bacteria types based on sterilization parameters was investigated on the surface of the load.

2. Experimental set up

Transient measurement data of the fluid temperature, the load temperature and the pressure during a sterilization cycle are required for validating the CFD results. The measurement data was obtained by using a commercially available benchtop steam sterilizer [16]. The steam sterilizer had a cylindrical shape with volume of 22 litre. On the back wall of the steam sterilizer a diffuser was mounted to distribute the steam within the steam sterilizer. On the opposite side of the steam sterilizer the door was mounted.

For the measurements of the fluid temperature, eight type-J thermocouples were evenly distributed within the steam sterilizer. The pressure inside the steam sterilizer was measured with one electronic pressure sensor [17]. The accuracy of the pressure sensor was given with $\pm$ 0.5%. The accuracy of all thermocouples (type J) used in this study was given with $\pm$ 1 K. The locations of the thermocouples T1, T4, T5 and T7 are depicted in Fig. 2. The location of all eight thermocouples and the location of the pressure sensor is described in a previous publication [13].

To guarantee sterile medical conditions for the purpose of storing or transporting the load is wrapped into pouches [18]. The pouch is made out of a special paper [19]. This study only investigated unwrapped load. For unwrapped load the steam is in direct contact with the load, and therefore responsible for the heating process of the load. To investigate all relevant phenomena on unwrapped load, in this study, the steam sterilizer was filled with eight cylinders placed on two trays (see Fig. 2). The cylinder materials were steel, aluminium, brass and plastic (ptfe). The cylinders had a diameter of approximately 25 mm and a length of 100 mm. The trays had a dimension of 380 mm $\times$ 186 mm x 2 mm and were made out of aluminium. To validate the heat transfer to the load, the load temperature was measured. Therefore, four thermocouples were placed in the center of the cylinders of the upper tray (see Fig. 2). This study progressed beyond the state-of-the-art by considering 1) the fluid temperature and the load temperature for unwrapped load.

3. Computational fluid dynamics (CFD)

CFD is a widely used method in the field of fluid mechanics. Numerical methods and algorithms are used to solve partial differential equations for velocity, pressure, energy, turbulence, and multiphase flow under given boundary conditions. The fluid region is subdivided into small control volumes (cells), known as a numerical grid. In this work, the steam sterilizer with the trays, the diffuser and the load were analyzed with approximately 550,000 polyhedron and hexahedron cells, including both the fluid and solid geometries of the steam sterilizer. The complete steam sterilizer was simulated due to the fact that the inlet is not in the symmetry plane of the sterilization chamber. Furthermore, the diffuser has no cylindrical shape. To get a better overview, the numerical grid is shown in Fig. 3. The fluid as well as the solids inside the steam sterilizer was finely resolved.

Past studies have shown that CFD is capable of predicting complex transport phenomena in the field of medicine [20–22]. Furthermore, previous works of Feurhuber et al. [13–15] showed that CFD is a useful tool to predict the complex flow inside steam sterilizers. The CFD model was extended to 1) predict the fluid temperature and the load temperature as well as the 2) steam quality inside a steam sterilizer for unwrapped load. Third, 3) the inactivation of the bacteria bacillus atrophaeus (Type 1) and the type bacillus subtilis (Type 2) was simulated on the surface of the load.

Simulations in this study were performed with ANSYS Fluent v19 [23]. The user defined functions (UDFs) were used for the definition of transient boundary conditions, for calculating the heat transfer to the load and for the calculation of the inactivation of the bacteria. All simulations were performed under transient conditions. Gravity was added to the CFD model to account for buoyancy. The complete sterilization phase of the investigated sterilization cycle (see blue arrow in Fig. 1) was simulated . This part of the sterilization cycle was selected due to the high levels of condensation as well as the high temperature gradients in the steam sterilizer as well as in the load. Furthermore, in

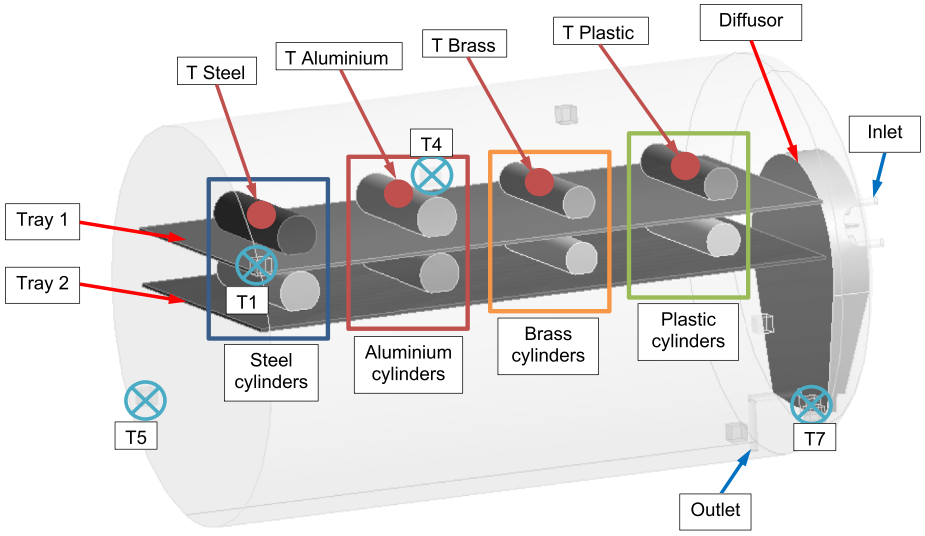

Fig. 2. Geometry of the CFD model with the unwrapped load and the locations of the measurements of the load temperature.

this part of the sterilization cycle, the main inactivation of the bacteria takes place.

3.1. Turbulence modeling

Modeling turbulence is a complex issue in the field of CFD. In the present work the realizable k-ε model by Shih et al. [24] was used to deal with the turbulent flow in the steam sterilizer. The realizable k-ε model solves one equation for the turbulent kinetic energy (k) and one equation for the turbulent dissipation (ε) to simulate the turbulence. The advantage of the realizable k-ε model is its numerical robustness and the fact that it shows substantially better results for free flows, rotating flows and channel flows compared to the standard k-ε model [23]. As a result, the realizable k-ε model is an often used turbulence model in industrial applications.

3.2. Evaporation and condensation model

A simple numerical technique, first published by Lee in 1980, was used in this paper [25]. Mass transfer due to evaporation (liquid phase to vapour phase) $\dot{m}_{lv}$ was considered in the model if the liquid temperature T_l exceeds the value of the saturation temperature T_{sat}.

$$\dot{m}_{lv} = r_v \cdot \alpha_l \cdot \rho_l \frac{T_l - T_{sat}}{T_{sat}} \tag{1}$$

In Eq. (1) α_l represents the volume fraction of the liquid phase and ρ_l

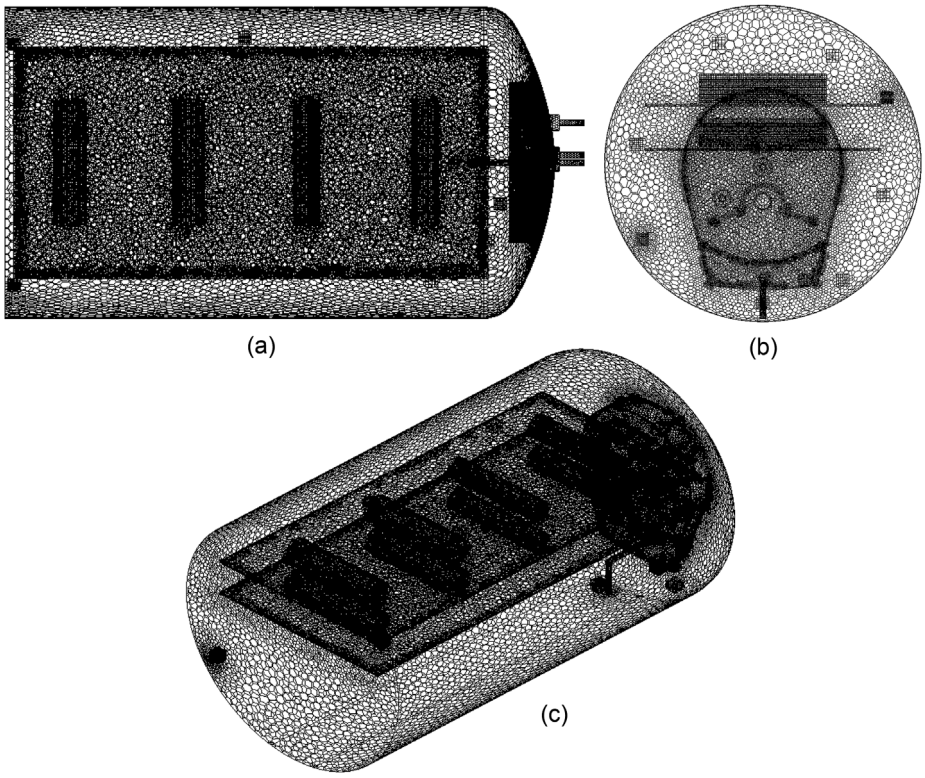

Fig. 3. (a) Top view of the numerically grid, (b) back view of the numerically grid and (d) a 3D-view of the numerical grid.

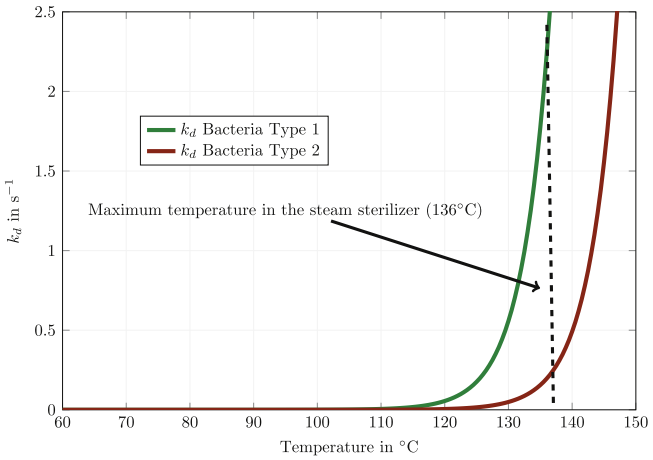

Fig. 4. k_d values for Bacteria Type 1 and Bacteria Type 2 over the temperature.

represents the density of the liquid phase. r_{lv} represents the evaporation coefficient of the Lee model. If the vapour temperature T_v is lower than the saturation temperature T_{sat} in any specific point within the steam sterilizer, then condensation takes place. The mass transfer for condensation (vapour phase to the liquid phase) $\dot{m}_{vl}$ is calculated in the following way (see Eq. (2)).

$$\dot{m}_{vl} = r_{vl} \cdot \alpha_v \cdot \rho_v \frac{T_{sat} - T_v}{T_{sat}} \tag{2}$$

The coefficients r_{lv} and r_{vl} are very sensitive depending on the respective case. The authors of this study carried out some individual experiments to investigate this coefficient. The condensation coefficient is similar to a frequency and describes the velocity at which the phase change takes place. In this study condensation coefficients r_{vl} were investigated for $2\ s^{-1}$, $20\ s^{-1}$, $200\ s^{-1}$, $2000\ s^{-1}$ and $10000\ s^{-1}$. The coefficient $r_{vl} = 200\ s^{-1}$ was found to match the experimental data very well. More details about the coefficients r_{lv} and r_{vl}, investigated for other flow regimes, can be found in the literature [25–28].

3.3. Modeling heat transfer

The modeling of the heat transfer is rather difficult in the CFD due to wall condensation. In order to reach the right heat transfer coefficients, a very fine mesh near the wall is necessary. Zschaeck et al. developed a model which was able to predict the heat transfer due do wall condensation [29]. Therefore, the authors decided to develop a numerically very efficient approach to calculate the heat transfer due to wall condensation. This model is based on an analytical approach. If the wall temperature is lower compared to the saturation temperature, the Nusselt number is multiplied by a factor. As a result, the heat transfer factor due to wall condensation can be calculated. More details about the developed heat transfer model can be found in the literature [13].

The big advantage of the developed heat transfer model is that the fluid flow inside the wall film which results from condensation must not be calculated. Therefore, no fine mesh near the wall is needed. The results in section 4.1, section 4.2 and section 4.3 show that the developed heat transfer model is able to predict the heat transfer and the condensation on the surface load.

3.4. Modeling the theoretical inactivation of bacteria

Two user defined scalars (UDS) were added to the commercial CFD code to simulate two strains of bacteria. The theoretical inactivation of the bacteria was modeled with a first order reaction kinematic approach. The integrated final equation of this approach is shown in Eq. (3).

$$N = N_0 \cdot e^{-k_d \cdot t} \tag{3}$$

where, N is the number of active bacteria, N_0 is the number of bacteria at the time $t = 0$ and k_d is the inactivation rate of the bacteria. In physical chemistry, the Arrhenius equation is often used to model the temperature dependence of reaction rates. In the past, it was found out that the inactivation rate of bacteria can also be modeled with the Arrhenius equation [30–32]. Therefore, the temperature dependence of the inactivation rate k_d in this study, was also modeled with the Arrhenius equation was used.

$$k_d = k_{d0} \cdot e^{\frac{-\Delta E_d}{R \cdot T_{(t)}}} \tag{4}$$

In Eq. (4), k_{d0} stands for the pre-exponential factor, whereas ΔE_d represents the activation energy of the bacteria type. R stands for the universal gas constant and $T_{(t)}$ stands for the temperature in Kelvin at a given time (t). In this study two different strains of bacteria were investigated. At first, the bacteria bacillus atrophaeus (Bacteria Type 1) was modeled. The reaction kinetics for this bacteria were taken from the work of Wallhäußer [32]. Secondly, the bacteria type of the work of P. De Santis and V.S. Rudo [33] (Bacteria Type 2) were investigated. Fig. 4 shows the inactivation rate k_d of the two investigated bacteria types as a function of the temperature. Furthermore, Table 1 shows the D-value of Bacteria Type 1 and of Bacteria Type 2. The D-value represents the exposure time (in minutes), which is needed to reduce 90% of the bacteria at a given temperature (T) [34]. The smaller the D-value, the faster the inactivation of the bacteria takes place. Generally, each bacteria type has its own specific D-value for steam sterilization. As can be seen in Fig. 4 and Table 1 Bacteria Type 1 represents a bacteria, which is easy to inactivate, whereas Bacteria Type 2 represents a bacteria, which is much more difficult to inactivate.

At the beginning of the simulation both types of were initialized with $N_0 = 10^{12}$, which represents an overkill value. An overkill value represents a cycle were more than 12-log of the investigated bacteria are inactivated. This value represents a possibility that one in a million items is not sterile (Sterility Assurance Level (SAL)) of 10^{-6}. More information about the modeling and the inactivation of bacteria, the overkill value and the SAL can be found in the literature [35, 36] and in guidelines [37].

3.5. Boundary conditions

In this model, a pressure inlet represents a 2100 W steam generator, which raises the pressure inside the steam sterilizer to the sterilization plateau (3.2 bar and 136 °C). The positioning of the inlet and the outlet can be seen in Fig. 2. According to measurements the steam at the inlet was saturated. The pressure and temperature of the steam at the inlet were also set to values based on measurements. In the simulated part of the sterilization cycle (see blue arrow in Fig. 1) all outlets are closed. All wall temperatures, as well as all load temperatures were calculated with the heat transfer model, described in section 3.3.

The heat losses were modeled with a convective boundary condition on the outer walls of the steam sterilizer. The free stream temperature was set according to the room temperature, which was approximately 298.15 K. The heat transfer coefficient on the outer walls was set to $5\ \frac{W}{m^2 K}$. The initial pressure, the initial fluid temperature as well as the initial temperature of the loads was set according to the measurements.

Table 1
D-values of the two investigated bacteria types.

	Bacteria Type 1	Bacteria Type 2
D-value for 111 °C	2.2 min	2.25 min
D-value for 121 °C	0.55 min	0.61 min

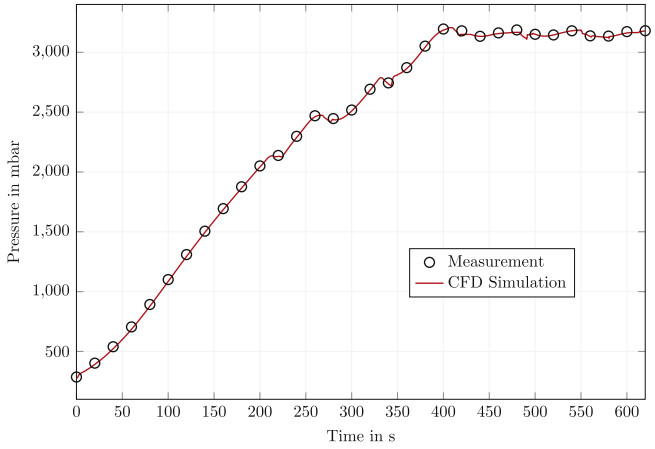

Fig. 5. Measured and simulated pressure inside the steam sterilizer.

Table 2
Absolute errors of the simulated fluid temperature on eight locations.

	After 205 s	After 300 s	After 410 s	After 620 s
Error T1	0.15%	0.02%	−0.10%	0.04%
Error T2	−0.55%	0.24%	0.16%	0.2%
Error T3	0.22%	0.25%	0.29%	0.21%
Error T4	0.16%	0.06%	0.19%	0.11%
Error T5	0.05%	0.09%	0.04%	0.05%
Error T6	−0.37%	0.05%	0.05%	0.06%
Error T7	−0.07%	0.18%	0.12%	0.38%
Error T8	0.14%	−0.19%	−0.25%	0.02%

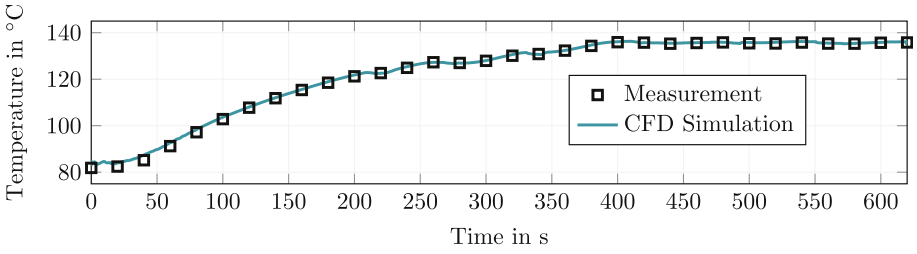

(a) Measured and simulated fluid temperature at the location of T1

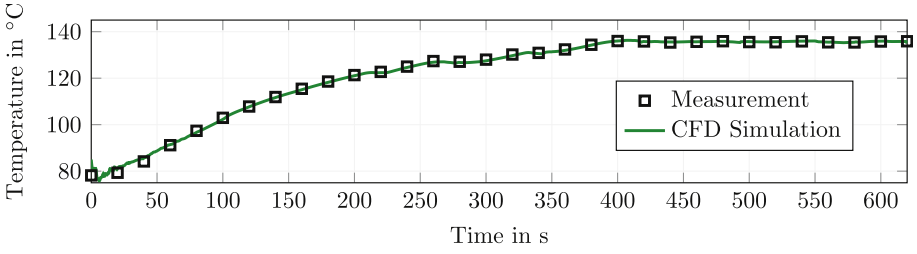

(b) Measured and simulated fluid temperature at the location of T4

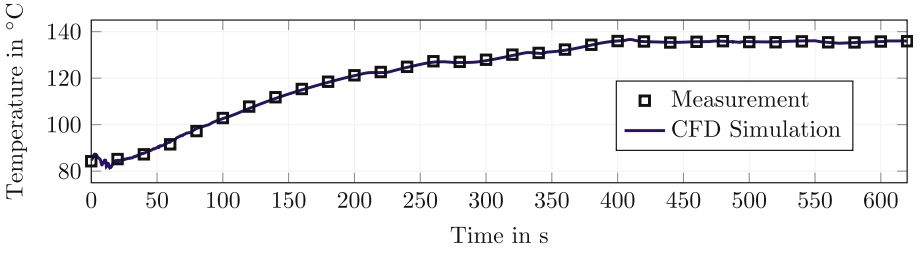

(c) Measured and simulated fluid temperature at the location of T5

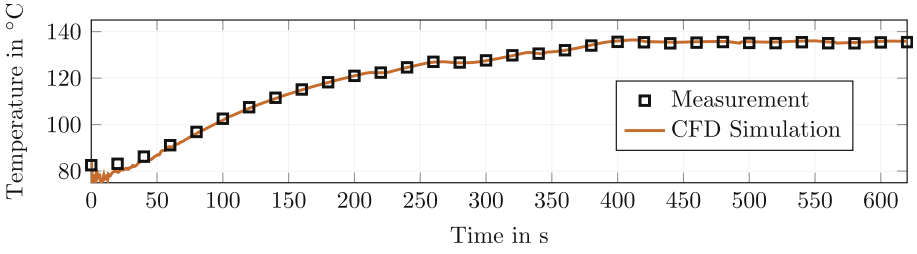

(d) Measured and simulated fluid temperature at the location of T7

Fig. 6. Measured and simulated fluid temperature at the locations (a) T1, (b) T4, (c) T5 and (d) T7.

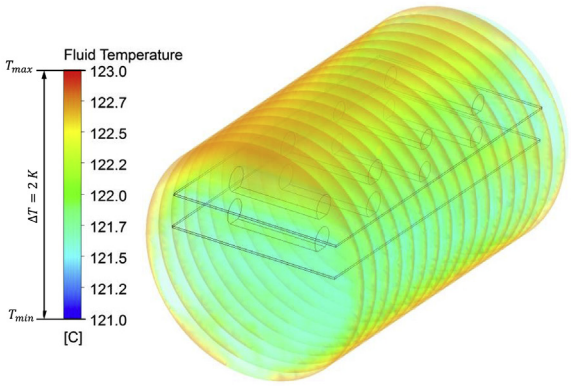

(a) Fluid temperature in the steam sterilizer after 205 s of simulation time

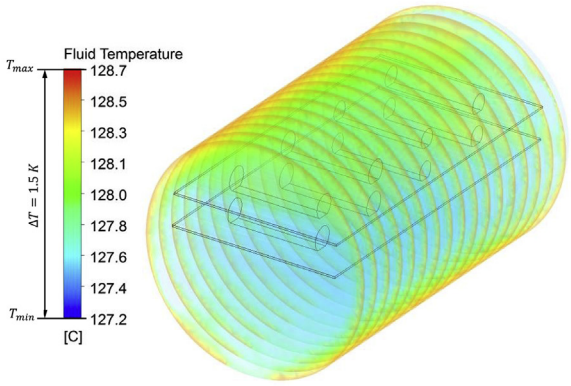

(b) Fluid temperature in the steam sterilizer after 300 s of simulation time

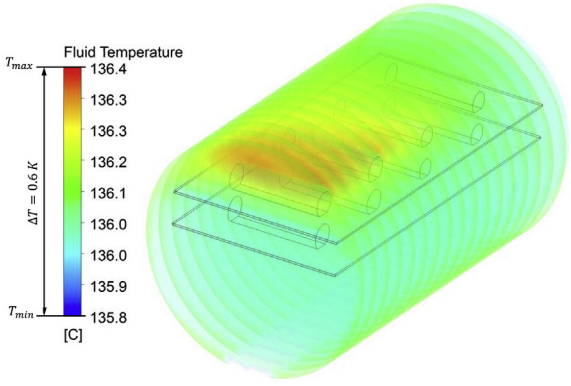

(c) Fluid temperature in the steam sterilizer after 410 s of simulation time

Fig. 7. Volume rendering of the fluid temperature in the steam sterilizer after (a) 205 s, (b) 300 s and (c) 410 s of simulation time.

4. Results

4.1. Pressure and fluid temperature in the steam sterilizer

The flow field of the CFD model was validated with measurements of one pressure sensor and eight thermocouples (type B) in the steam sterilizer. The thermocouples were represented in the CFD model using small volumes. Furthermore, an identical volume was created to compare the measured pressure with the simulated one. The diameter of the thermocouples was 1 mm. The simulation starts at the beginning of the sterilization phase (0.29 bar, 82 °C) and ends at the end of the sterilization phase (approximately, 3.2 bar and 136 °C, see blue arrow in Fig. 1).

Fig. 5 shows the measured and simulated pressure inside the steam sterilizer. It can be seen that the measured and the simulated pressure are in very good accordance, due to the fact that the average error between the simulated and the measured pressure is below 0.5%, which is below the accuracy of the pressure sensor. The maximum error between the measured and the simulated pressure is below 2%. In Fig. 6, the temperatures calculated and measured by four thermocouples during the simulated part of the sterilization cycle can be seen. In this study, the temperatures of thermocouples T1, T4, T5 and T7 are compared with the simulated temperatures. The locations of the thermocouples can be seen in Fig. 2. Furthermore, the measured and simulated fluid temperatures are compared for the other four thermocouples (T2, T3, T6 and T8) as well, indicating similar results. The results indicate that the measured fluid temperatures are in a very good accordance with the simulated fluid temperatures. To show the accuracy of the CFD model the error between the measured and simulated temperatures was calculated for different cycle times (see Eq. (5)).

$$Error = \left(1 - \frac{T_{Measurement}}{T_{Simulation}}\right) \cdot 100\ \% \tag{5}$$

In this equation $T_{Measurement}$ is the measured temperature and $T_{Simulation}$ is the simulated temperature in Kelvin. The absolute errors of all eight thermocouples for 205 s, 300 s, 410 s and 620 s of simulation time are shown in Table 2. The times where the errors are calculated are shown with blue vertical doted lines in Fig. 1. The biggest error with a value of 0.55% is detected after 205 s on the location of T2. Nevertheless, this error is still negligible, as the average error is below 0.2%. These results indicate that the developed CFD model is able to predict the fluid temperature inside the steam sterilizer.

After the validation of the simulated fluid temperature, the temperature distribution inside the steam sterilizer was investigated using CFD. Therefore, volume renderings of the fluid temperature inside the steam sterilizer are shown in Fig. 7. Fig. 7(a) shows the fluid temperature after 205 s. The maximum temperature differences detected at this time are 2 K. As is to be expected, the temperature difference decreases as the cycle goes on. After 410 s of simulation time the temperature stratification inside the steam sterilizer is below 0.6 K (see Fig. 7(c)). These results indicate that the investigated benchtop steam sterilizer [16] works very well. The temperature distribution inside the steam sterilizer is homogeneously (as can be seen in Fig. 7(c)). After 450 s of simulation time the temperature difference inside the steam sterilizer is below 0.5 K. The coldest spots are detected in the middle of the steam sterilizer under the second tray for all investigated cycle times. It is proven that with 1) CFD it is possible to predict the fluid temperature and the pressure within the steam sterilizer for unwrapped load.

4.2. Temperature of the unwrapped load

In order to understand the full sterilization process, it is essential to have thorough knowledge of the load temperature and of what constitutes sufficient process time. To reach sterility, high wall temperatures are required. To validate the predicted heat transfer of the CFD model to the load and vice versa, simulated load temperatures were compared with measured load temperatures. The temperature at the center of all eight cylinders was recorded. Position and material of the load cylinders can be seen in Fig. 2. As can be seen in Fig. 8, the simulated load temperatures are in very good accordance with the measured load temperatures throughout the investigated phase. Calculated temperatures for steel (a), aluminum (b), brass (c) and plastic (d) are in good accordance.

To predict the inactivation of bacteria, the surface temperature of the load is of high interest. Fig. 9 shows the surface load temperature

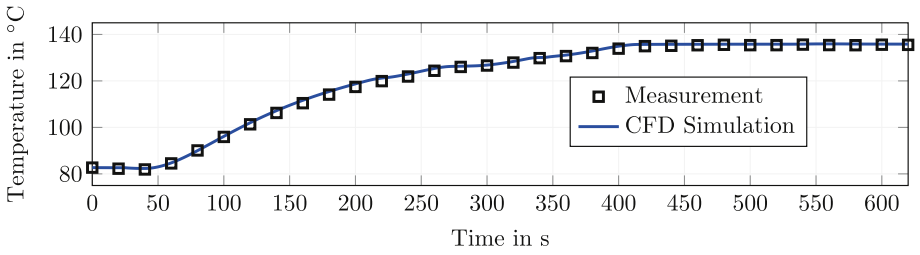

(a) Measured and simulated temperature in the center of the steel cyclinder

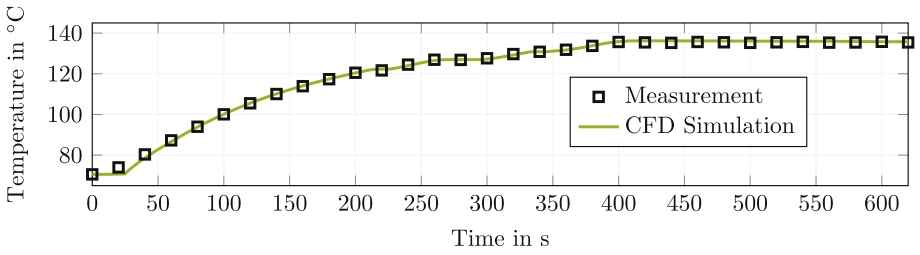

(b) Measured and simulated temperature in the center of the aluminium cyclinder

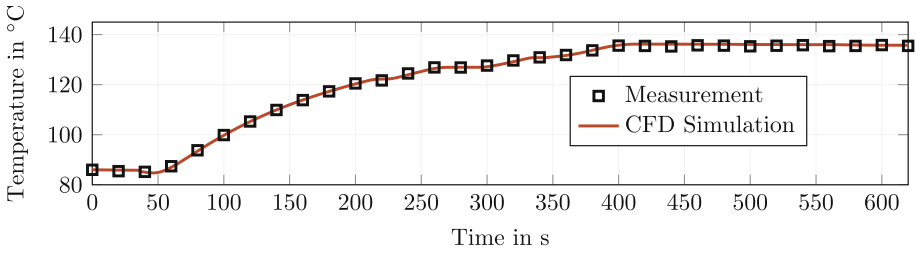

(c) Measured and simulated temperature in the center of the brass cyclinder

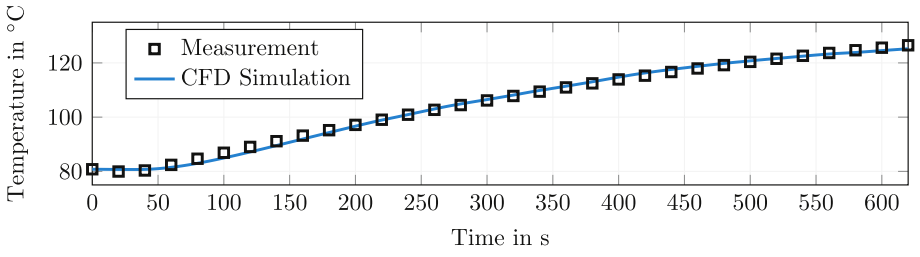

(d) Measured and simulated temperature in the center of the plastic cyclinder

Fig. 8. Measured and simulated temperature in the center of the (a) steel cylinder, (b) aluminum cylinder, (c) brass cylinder and (d) the plastic cylinder.

after (a) 205 s, (b) 410 s and (c) 620 s of simulation time. After 200 s of simulation time the lowest surface temperatures are to be found on the steel cylinders (see Fig. 9(a)). This can be explained through higher mass, compared to the other cylinders. After 620 s of cycle time the temperature difference on the surface of the load decreases under 0.3 K. Highest temperatures are detected on the edges of the cylinders (see Fig. 9(c)). This small temperature differences can have a big influence on the inactivation of the bacteria, due to the fact that the inactivation rate of the bacteria k_d is an exponential factor of the temperature (see Eq. (4)).

These results prove that the 1) developed CFD model is able to predict the heat transfer to the unwrapped load in an accurate way. Similar results were found in a previous publication for wrapped load [13]. Furthermore, in this and a previous publication [13] demonstrated that the influence of the wrapping on the load temperature is negligible. This means that the wrapping of an load does not influence the load temperature. Only the steam quality near the load and inside the steam sterilizer is influenced by the wrapping (see section 4.3).

4.3. Steam quality

The steam quality in the steam sterilizer is of interest due to the fact that a low steam quality decreases the heat transfer due to wall condensation [38]. The steam quality (x) is defined by dividing the mass of the saturated steam ($m_{saturated\ steam}$) through the mass of the wet steam ($m_{wet\ steam}$) (see Eq. (6)):

$$x = \frac{m_{saturated\ steam}}{m_{wet\ steam}} = \frac{m''}{m' + m''} \tag{6}$$

where m' stands for the mass of the boiling water and m'' for the mass of the saturated steam. According to this definition saturated steam is represented with a steam quality of $x = 1$ and boiling water is represented with a steam quality of $x = 0$.

Due to the fact that it is quite difficult to measure the steam quality in the steam sterilizer, CFD calculations were used to investigate this issue. In this study 2) the steam quality was investigated for unwrapped load. The simulated steam quality is shown on four planes in the steam

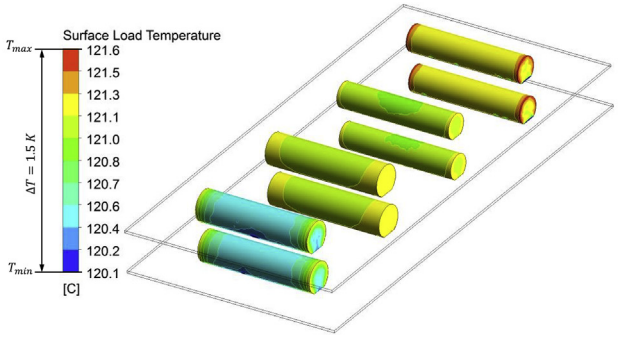

(a) Simulated surface temperature of the unwrapped load after 205 s of simulation time

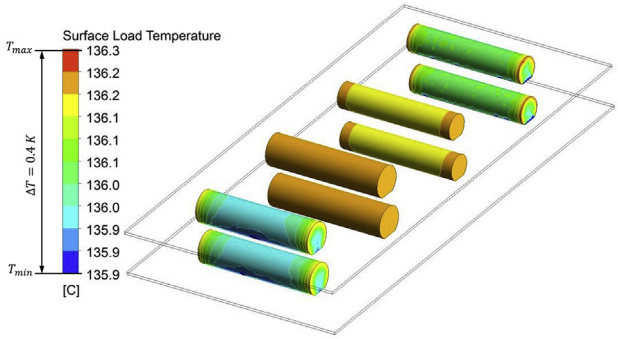

(b) Simulated surface temperature of the unwrapped load after 410 s of simulation time

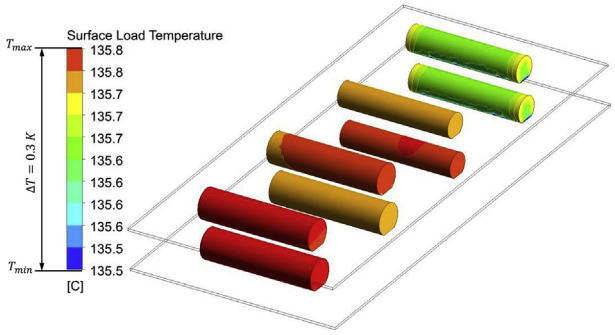

(c) simulated surface temperature of the unwrapped load after 620 s of simulation time

Fig. 9. Simulated surface temperature of the unwrapped load after (a) 205 s, (b) 410 s and (c) 620 s of cycle time.

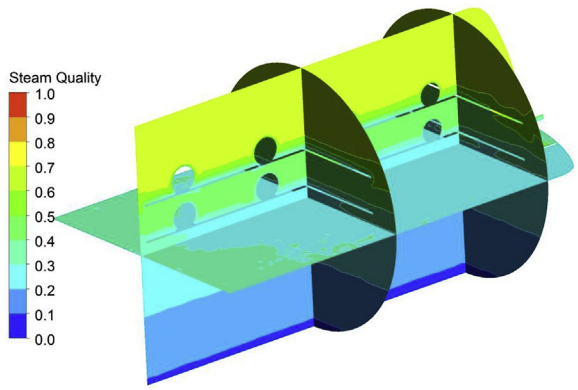

(a) Steam quality in the steam sterilizer after 205 s of simulation time

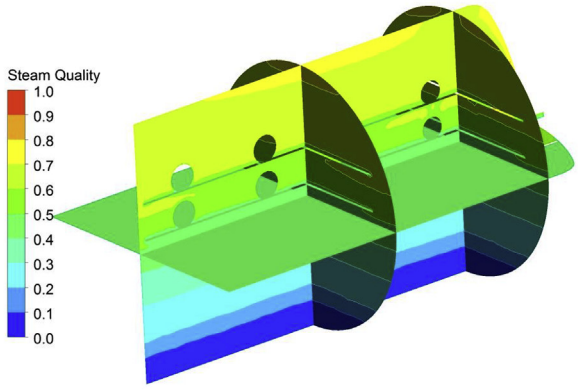

(b) Steam quality in the steam sterilizer after 410 s of simulation time

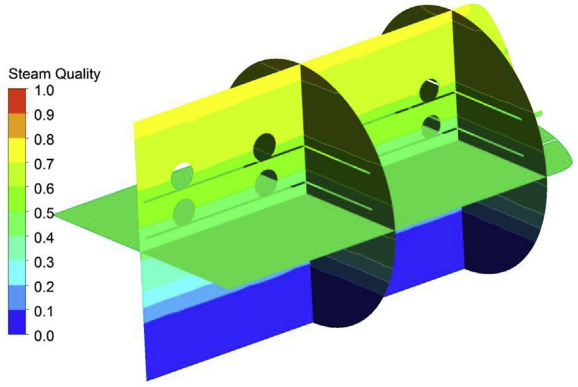

(c) Steam quality in the steam sterilizer after 620 s of simulation time

Fig. 10. Steam quality in the steam sterilizer after (a) 205 s, (b) 410 s and (c) 620 s of simulation time.

sterilizer. Those planes are the vertical middle surface, the horizontal middle surface and two radial planes. The latter two can be found half way through and near the back of the steam sterilizer. Upon examination of additional radial planes, no further differences are found. The lowest quality steam is found in the bottom region of the steam sterilizer (see Fig. 10) due to the fact of buoyancy effects. Furthermore, the results show that the volume fraction of the steam quality decreases with increasing cycle time (see Fig. 10). In a previous publication the steam quality was investigated for wrapped load [13]. The results of that study show that the average steam quality in the steam sterilizer improves if the load is wrapped, whereas the average steam quality near the load improves if the load is unwrapped. Nevertheless, hardly any differences regarding the surface temperature of the load are found between wrapped load [13] and unwrapped load (this study). This indicates that both wrapping the load and the steam quality have a negligible impact, due to the fact that high heat transfer rates to the load are present in every case.

Without the developed heat transfer model it would not be possible to calculate the heat transfer to the load and the chamber of the steam sterilizer (described in section 3.3). As a result the condensation would not be predicted correctly and therefore it would not be possible to predict the steam quality inside the steam sterilizer.

4.4. Prediction of the theoretical active bacteria on the load

The aim of a steam sterilization cycle is to reach a high enough kill-ratio of the bacteria that the chance of a contamination is minimized. According to guidelines a steam sterilization process should reach a SAL of 10^{-6} [37]. This SAL represents the probability that one out of a million items is contaminated. To investigate the kill-ratio, the authors

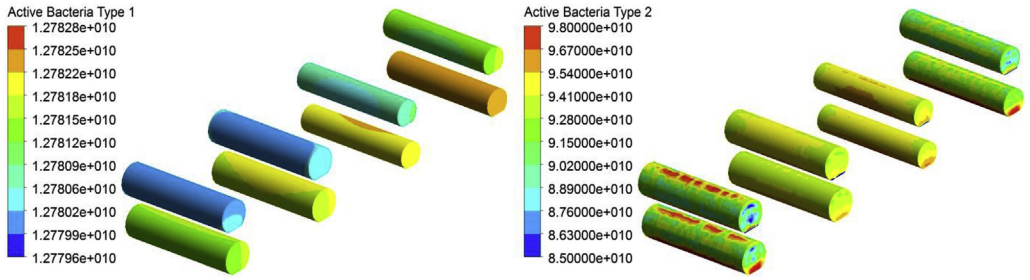

(a) Active bactera of Type 1 (left) and Type 2 (right) after 205 s of simulation time

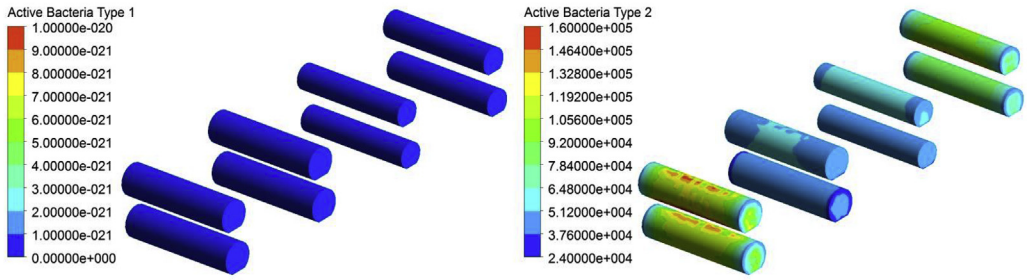

(b) Active bactera of Type 1 (left) and Type 2 (right) after 410 s of simulation time

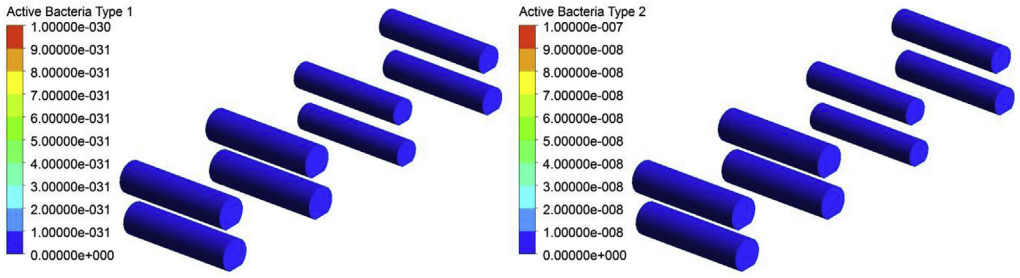

(c) Active bactera of Type 1 (left) and Type 2 (right) after 620 s of simulation time

Fig. 11. Active bacteria of the two investigated types on the surface of the unwrapped load after (a) 205 s, (b) 410 s and (c) 620 s of simulation time.

Table 3
Log survival ratio for Bacteria Type 1 and Bacteria Type 2 for different simulation times.

	log survival ratio of Bacteria Type 1	log survival ratio of Bacteria Type 2
After 205 s	−1.89	−1.12
After 410 s	−33.95	−6.45
After 620 s	−50.96	−22.21

developed a 3) CFD model that is able to predict the theoretical active bacteria in every point of the steam sterilizer resolved in time and space. Two different types of bacteria were investigated (Bacteria Type 1 and bacteria Type 2). More about the modeling of the inactivation and the inactivation rates k_d of the investigated bacteria types can be found in section 3.4. The active bacterias of Type 1 and Type 2 for the simulation times 205 s, 410 s and 620 s can be seen in Fig. 11. The inactivation rate of Bacteria Type 1 is significant higher for every temperature compared to the inactivation rate of Bacteria Type 2 (see Fig. 4). For example, at 136 ° the inactivation rate of Bacteria Type 1 is 2.3 s^{-1}, whereas the inactivation rate of Bacteria Type 2 is 0.2 s^{-1}. As a result the inactivation of the Bacteria of Type 1 takes less time. At the end of the pressure rise in the sterilization phase (410 s), hardly any active Type 1 bacteria remain (see Fig. 11(c)). At the same time, approximately one third of Type 2 bacteria are still active. It can also be seen that the regions with the lowest surface temperatures are the same regions where the most bacteria are still active (see surface of the steel cylinder in Figs. 9 and 11).

To get a better understanding of the inactivation of the log survival ratio is often used. The definition of the log survival ratio is given by:

$$log\ survival\ ratio = log\frac{N}{N_0} \tag{7}$$

Table 3 shows the surface average log reduction values of the steel cylinders for 205 s, 410 s, and 620 s of simulation time. As expected, this log reduction ratio is significantly higher for Bacteria Type 1 compared to Bacteria Type 2. After 410 s approximately 33 log ratios are inactivated for Bacteria Type 1, whereas approximately 6.45 log ratios are inactivated for Bacteria Type 2. Nevertheless, at the end of the simulated phase of the steam sterilization cycle (620 s) hardly any bacteria of Type 1 and Type 2 are active (see Fig. 11(c). The log reduction of Bacteria of Type 1 at the end of the sterilization phase (620 s) is approximately 51, for Bacteria Type 2 approximately 22, respectively (see Table 3). The same results were found for wrapped load in a previous publication [13].

These and results from a previous publication [13] indicate that it is possible to predict the theoretical inactivation of different types of bacteria based on sterilization parameters, on the surface of the wrapped load, as well as on the surface of unwrapped load using CFD. Nevertheless, the developed heat transfer model described in section 3.3 is the key for these kind of CFD simulations.

5. Conclusion

This paper presents a CFD model that was developed for a steam sterilizer and is capable of calculating all of the essential processes therein. The application of this model 1) makes it possible to predict the fluid flow and temperature distribution, as well as mass transfer between steam and water, during the sterilization cycle of an unwrapped load, 2) allows to calculate the steam quality inside the steam sterilizer for unwrapped load. Furthermore, 3) the theoretical inactivation of two different bacteria types was accurately predicted in the steam sterilizer was well as on the surface of the unwrapped load.

To validate the simulation results, the pressure as well as the temperature in the steam sterilizer were measured and compared with simulated values. The measured pressure, as well as the measured fluid temperature were in very good accordance for different locations in the steam sterilizer. Differences between the measured and the simulated temperatures were below 0.4 K. Additionally, measurements of the load temperature were performed. A heat transfer model was developed to calculate the heat transfer to the load which results from wall condensation. Results show that the developed heat transfer model is able to calculate the heat transfer to the load with high accuracy.

Furthermore, two first order reaction kinetic approaches were added to the CFD model to calculate the theoretical inactivation of two different types of bacteria based on sterilization parameters, in the steam sterilizer as well as on the surface of the load. With the CFD model developed in this study, the theoretical inactivation of any bacteria type can be investigated for any steam sterilization cycle. The theoretical inactivation of bacteria based on sterilization parameters can be predicted on the surface of medical devices, as well as in the hollow volumes of medical equipment. This knowledge can lead to big improvements for developers as well as users of steam sterilizers.

Future works will address the microbiological validation of the simulated theoretical inactivation of bacteria. In the current work the theoretical inactivated bacteria are based on available reaction kinetic approaches from the literature. To improve the used reaction kinetic model shorter cycles can be simulated and validated against measurements with spore stripes. With this validation, it will be possible to simulate the real inactivation of bacteria.

This and other studies [39–42] demonstrate that physical approaches have a big potential in the field of medicine due to the fact that with reported experimental and numerical simulations a deep timely and spatially insight inside medical processes is possible to obtain.

References

[1] 285:2006 + A2:2009, B.E. BS EN 285:2006 + A2:2009, Sterilization. Steam sterilizers. Large sterilizers – BSI British Standards, http://shop.bsigroup.com/ProductDetail/?pid=000000000030192330, (2009).

[2] EN 13060:2004 - Small Steam Sterilizers, (2004).

[3] 17665-1:2006(en), I. ISO 17665-1:2006(en), Sterilization of health care products — moist heat — Part 1: requirements for the development, validation and routine control of a sterilization process for medical devices, https://www.iso.org/obp/ui/iso:std:iso:17665:-1:ed-1:v1:en, (2006).

[4] G. Caruso, D. Vitale Di Maio, A. Naviglio, Condensation heat transfer coefficient with noncondensable gases inside near horizontal tubes, Desalination 309 (Supplement C) (2013) 247–253, https://doi.org/10.1016/j.desal.2012.10.026 http://www.sciencedirect.com/science/article/pii/S0011916412005838.

[5] N. Lapanaitis, L. Frizzell, A. Downing, J. Van Doornmalen, Case study: correlation between the duration of a steam sterilization process and the weight of the processed load, Zentralsterilisation – Cent. Serv. 26 (4) (2018) 225–230.

[6] J. Grömann, U. Kaiser, R. Menzel, Entlüftungsverhalten von unterschiedlichen Dampf-Sterilisationsprozessen gegenüber porösen und hohlen Sterilisiergütern, Zentralsterilisation – Cent. Serv. 9 (3) (2001) 177–186.

[7] U. Kaiser, J. Göman, Investigations of air removal from hollow devices in steam sterilisation processes, Zentralsterilisation – Cent. Serv. 6 (6) (1998) 401–413.

[8] A. De Bruijn, A. Van Drongelen, Performance evaluation of hispital steam sterilizers using the european helix test, Zentralsterilisation – Cent. Serv. 13 (5) (2005) 330–336 13.

[9] U. Kaiser, Simple method to assess efficacy of sterilisation processes for hollow instruments, Zentralsterilisation – Cent. Serv. 7 (6) (1999) 393–395.

[10] U. Kaiser, Auswirkungen von nicht-kondensierbaren Gasen (NKG) in Dampfsterilisationsprozessen, Zentralsterilisation – Cent. Serv. 13 (2005) 45–47.

[11] W.L. Lau, J. Reizes, V. Timchenko, S. Kara, B. Kornfeld, Heat and mass transfer model to predict the operational performance of a steam sterilisation autoclave including products, Int. J. Heat Mass Transf. 90 (2015) 800–811, https://doi.org/10.1016/j.ijheatmasstransfer.2015.06.089 http://www.sciencedirect.com/science/article/pii/S0017931015007103.

[12] W.L. Lau, J. Reizes, V. Timchenko, S. Kara, B. Kornfeld, Numerical modelling of an industrial steam–air sterilisation process with experimental validation, Appl. Therm. Eng. 75 (2015) 122–134, https://doi.org/10.1016/j.applthermaleng.2014.09.031 http://www.sciencedirect.com/science/article/pii/S1359431114008035.

[13] M. Feurhuber, A. Cattide, M. Magno, M. Miranda, R. Prieler, C. Hochenauer, Prediction of the fluid flow, heat transfer and inactivation of microorganism at medical devices in modern steam sterilizers using computational fluid dynamics, Appl. Therm. Eng. 127 (2017) 1391–1403, https://doi.org/10.1016/j.applthermaleng.2017.08.085 http://www.sciencedirect.com/science/article/pii/S1359431117330739.

[14] M. Feurhuber, M. Magno, M. Miranda, C. Hochenauer, CFD investigations of steam penetration, air-removal and condensation inside hollow loads and cavities, Appl. Therm. Eng. 147 (2019) 1070–1082, https://doi.org/10.1016/j.applthermaleng.2018.10.135 http://www.sciencedirect.com/science/article/pii/S1359431118344120.

[15] M. Feurhuber, M. Magno, M. Miranda, R. Prieler, C. Hochenauer, CFD investigation of non-condensable gases in vacuum and non-vacuum steam sterilizers, Chem. Ing. Tech. 91 (4) (2019) 1–13, https://doi.org/10.1002/cite.201800088 https://onlinelibrary.wiley.com/doi/abs/10.1002/cite.201800088.

[16] W&H Lisa, Instruction for use, Available at: http://www.wh.com/backend/Document.mvc/Download?documentId=1400011-AEN00&filename=Lisa%2bva131%2beng%2brev04%2buser%2bmanual.pdf.

[17] Pressure transmitter for general industrial applications Model A-10, Data sheet, Available at https://www.wika.co.uk/upload/DS_pe8160_en_co_1631.pdf.????.

[18] EC (European Commission), EC guidelines of good manuf acturing practice for medical products, Pharm. Ind. (Pharmind) 52 (1990) 853–874 (????).

[19] Euronda, Technical data sheet, Available at https://www.euronda.de/media/pdf/12/05/0d/euronda-tdb-eurosteril.pdf.????.

[20] P.L. Yuen, R. Yam, R. Yung, K.L. Choy, Fast-track ventilation strategy to cater for pandemic patient isolation surges, J. Hosp. Infect. 81 (4) (2012) 246–250, https://doi.org/10.1016/j.jhin.2012.04.013 http://www.sciencedirect.com/science/article/pii/S0195670112001156.

[21] R. Yam, P.L. Yuen, R. Yung, T. Choy, Rethinking hospital general ward ventilation design using computational fluid dynamics, J. Hosp. Infect. 77 (1) (2011) 31–36, https://doi.org/10.1016/j.jhin.2010.08.010 http://www.sciencedirect.com/science/article/pii/S0195670110004032.

[22] A.M. Fic, D.B. Ingham, M.K. Ginalski, A.J. Nowak, L. Wrobel, Heat and mass transfer under an infant radiant warmer—development of a numerical model, Med. Eng. Phys. 32 (5) (2010) 497–504, https://doi.org/10.1016/j.medengphy.2010.02.021 http://www.sciencedirect.com/science/article/pii/S1350453310000500.

[23] ANSYS Fluent Theory Guide, (2016).

[24] T.H. Shih, W.W. Liou, A. Shabbir, Z. Yang, J. Zhu, A new k-ε eddy viscosity model for high Reynolds number turbulent flows, Comput. Fluid 24 (3) (1995) 227–238, https://doi.org/10.1016/0045-7930(94)00032-T http://www.sciencedirect.com/science/article/pii/004579309400032T.

[25] W. Lee, A pressure iteration scheme for two-phase flow modeling, in: T.N. Veziroglu (Ed.), Multiphase Transport Fundamentals, Reactor Safety, Applications, 1 Hemisphere Publishing, Washington, DC, 19801980 https://www.researchgate.net/publication/291211634.

[26] E. Da Riva, D. Del Col, Numerical simulation of laminar liquid film condensation in a horizontal circular minichannel, J. Heat Transf. 134 (5) (2012), https://doi.org/10.1115/1.4005710 051019-051019.

[27] Z. Yang, X.F. Peng, P. Ye, Numerical and experimental investigation of two phase flow during boiling in a coiled tube, Int. J. Heat Mass Transf. 51 (5) (2008) 1003–1016, https://doi.org/10.1016/j.ijheatmasstransfer.2007.05.025 http://www.sciencedirect.com/science/article/pii/S001793100700405X.

[28] G. Qiu, W. Cai, Z. Wu, Y. Yao, Y. Jiang, Numerical simulation of forced convective condensation of propane in a spiral tube, J. Heat Transf. 137 (4) (2015), https://doi.org/10.1115/1.4029475.

[29] G. Zschaeck, T. Frank, A.D. Burns, CFD modelling and validation of wall condensation in the presence of non-condensable gases, Nucl. Eng. Des. 279 (2014) 137–146, https://doi.org/10.1016/j.nucengdes.2014.03.007 http://www.sciencedirect.com/science/article/pii/S0029549314001393.

[30] M.S. Hossain, N.N.N.A. Rahman, V. Balakrishnan, Z.A. Rajion, M.O. Ab Kadir, Mathematical modeling of Enterococcus faecalis, Escherichia coli, and Bacillus sphaericus inactivation in infectious clinical solid waste by using steam autoclaving and supercritical fluid carbon dioxide sterilization, Chem. Eng. J. 267 (2015) 221–234, https://doi.org/10.1016/j.cej.2014.07.097 http://www.sciencedirect.com/science/article/pii/S1385894714009929.

[31] Wang, D.I.C., Scharer, J., Humphrey, A.E. Kinetics of death of bacterial spores at elevated temperatures. Appl. Microbiol.;:4.

[32] K.H. Wallhäußer, Praxis der Sterilisation, Desinfektion, Konservierung : Keimidentifizierung, Betriebshygiene. 4. überarbeitete und erweiterte Auflage. Thieme, (1988).

[33] P. De Santis, V.S. Rudo, Validation of steam sterilization in autoclaves, in: F.J. C a r l e t o n, J.P. Agalloco (Eds.), Validation of Aseptic Pharmaceutical Processes, 2d ed., Marcel Dekker, New York, 1986, pp. 279–317 1986.

[34] P.G. Mazzola, T.C.V. Penna, A.M. da S Martins, Determination of decimal reduction time (D value) of chemical agents used in hospitals for disinfection purposes, BMC

Infect. Dis. 3 (2003) 24, https://doi.org/10.1186/1471-2334-3-24 https://www.ncbi.nlm.nih.gov/pmc/articles/PMC270032/.
[35] P. Deinhard, U. Kaiser, H. Keßler, Test method to determine the microbiological resistance and characterization of the reaction kinetics of hydrogen peroxide sterilization processes, Central Serv. 03 (03/2016) (2016) 171–176.
[36] D. Haider, J. Göman, U. Junghannß, U. Kaiser, Kill kinetics study of Bacillus subtilis spores in ethylene oxide sterilisation processes, Zentral Sterilis. 10 (3) (2002) 158–167.
[37] C.f.D.a.R. Health, Reprocessing medical devices in health care settings: validation methods and labeling, http://www.fda.gov/regulatory-information/search-fda-guidance-documents/reprocessing-medical-devices-health-care-settings-validation-methods-and-labeling, (2019).
[38] G. Qiu, X. Wei, W. Cai, Y. Jiang, Development and validation of numerical model of condensation heat transfer and frictional pressure drop in a circular tube, Appl. Therm. Eng. 143 (2018) 225–235, https://doi.org/10.1016/j.applthermaleng.2018.07.085 http://www.sciencedirect.com/science/article/pii/S1359431118301741.
[39] M. Khorshid, P. Losada-Pérez, G. Wackers, D. Yongabi, F.U. Renner, R. Thoelen, et al., Real-time monitoring of interactions between Ebola fusion peptide and solid-supported phospholipid membranes: effect of peptide concentration and layer geometry, Phys. Med. 4 (2017) 1–7, https://doi.org/10.1016/j.phmed.2017.06.001 http://www.sciencedirect.com/science/article/pii/S2352451017300033.
[40] H.Y. Yacoob Aldosky, A. Yildiz, H.A. Hussein, Regional body fat distribution assessment by bioelectrical impedance analysis and its correlation with anthropometric indices, Phys. Med. 5 (2018) 15–19, https://doi.org/10.1016/j.phmed.2018.02.001 http://www.sciencedirect.com/science/article/pii/S2352451017300161.
[41] H.S. Gill, B. Elshahat, A. Kokil, L. Li, R. Mosurkal, P. Zygmanski, et al., Flexible perovskite based X-ray detectors for dose monitoring in medical imaging applications, Phys. Med. 5 (2018) 20–23, https://doi.org/10.1016/j.phmed.2018.04.001 http://www.sciencedirect.com/science/article/pii/S2352451018300088.
[42] K. Betlem, S. Hoksbergen, N. Mansouri, M. Down, P. Losada-Pérez, K. Eersels, et al., Real-time analysis of microbial growth by means of the Heat-Transfer Method (HTM) using Saccharomyces cerevisiae as model organism, Phys. Med. 6 (2018) 1–8, https://doi.org/10.1016/j.phmed.2018.05.001 http://www.sciencedirect.com/science/article/pii/S235245101830009X.